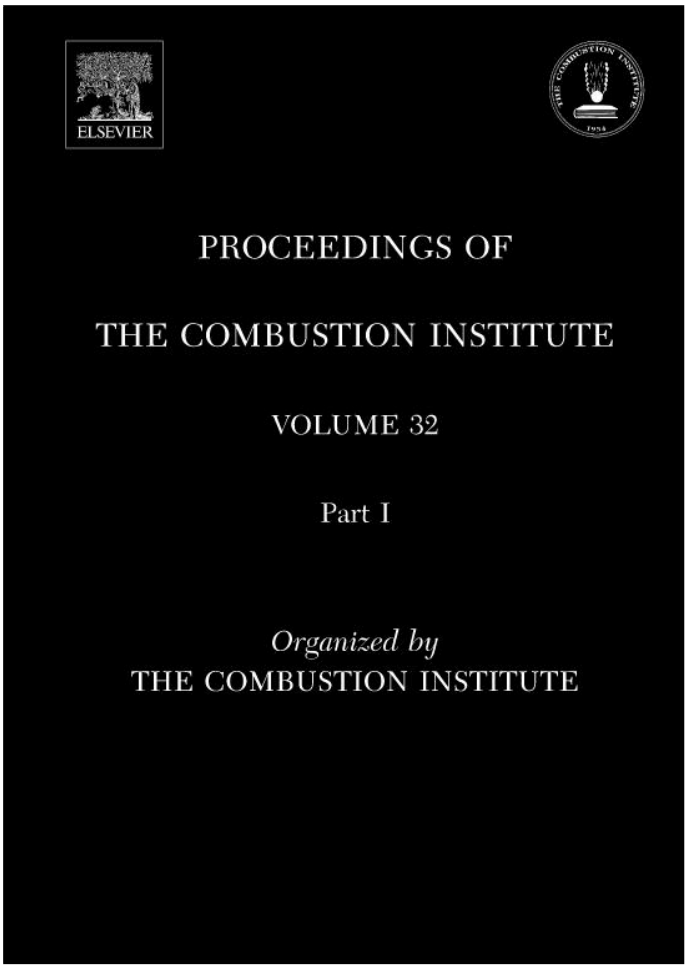

Available online at www.sciencedirect.com
ScienceDirect
Proceedings of the Combustion Institute 32 (2009) 279–286
Proceedings of the Combustion Institute
www.elsevier.com/locate/proci

Theoretical rate coefficients for the reaction of methyl radical with hydroperoxyl radical and for methylhydroperoxide decomposition

Ahren W. Jasper [a,*], Stephen J. Klippenstein [b], Lawrence B. Harding [b]

[a] *Combustion Research Facility, Sandia National Laboratories, P.O. Box 969, Livermore, CA 94551, USA*
[b] *Chemistry Division, Argonne National Laboratory, Argonne, IL 60439, USA*

Abstract

The kinetics of the $CH_3 + HO_2$ bimolecular reaction and the thermal decomposition of CH_3OOH are studied theoretically. Direct variable reaction coordinate transition state theory (VRC-TST), coupled with high level multireference electronic structure calculations, is used to compute capture rates for the $CH_3 + HO_2$ reaction and to characterize the transition state of the barrierless $CH_3O + OH$ product channel. The $CH_2O + H_2O$ product channel and the $CH_3 + HO_2 \rightarrow CH_4 + O_2$ reaction are treated using variational transition state theory and the harmonic oscillator and rigid rotor approximations. Pressure dependence and product branching in the bimolecular and decomposition reactions are modeled using master equation simulations. The predicted rate coefficients for the major products channels of the bimolecular reaction, $CH_3O + OH$ and $CH_4 + O_2$, are found to be in excellent agreement with values obtained in two recent modeling studies. The present calculations are also used to obtain rate coefficients for the $CH_3O + OH$ association/decomposition reaction.

Keywords: Methylhydroperoxide; Methyl radical; Hydroperoxyl radical; Ab initio; Barrierless kinetics

1. Introduction

In some combustion systems at moderate temperatures and high pressures, the stabilization of $H + O_2$ to form hydroperoxyl radicals is favored over explosive chain branching, and CH_3 and HO_2 are the dominant species in the radical pool. The $CH_3 + HO_2$ reaction competes with methyl self-recombination as the major sink for CH_3. The relative significance of these pathways for CH_3 consumption has important consequences, as the hydroperoxyl reaction produces the reactive species OH and H, whereas the self-recombination reaction is chain terminating [1]. For example, in a modeling study of CH_4/O_2 at high pressures, the $CH_3 + HO_2$ reaction was found to be an important source of OH during ignition, and the authors identified this reaction as one requiring further study [2].

The bimolecular reaction of methyl radical and hydroperoxyl radical may proceed indirectly via an energized complex

$$CH_3 + HO_2 \rightarrow CH_3OOH^*(+M) \rightarrow CH_3O + OH \quad (1a)$$
$$\rightarrow CH_2O + H_2O \quad (1b)$$
$$\rightarrow CH_3OOH \quad (1c)$$

* Corresponding author. Fax: +1 925 294 2276.
E-mail address: ajasper@sandia.gov (A.W. Jasper).

1540-7489/$ - see front matter © 2009 The Combustion Institute. Published by Elsevier Inc. All rights reserved.
doi:10.1016/j.proci.2008.05.036

or via hydrogen abstraction

$$CH_3 + HO_2 \rightarrow CH_4 + {}^3O_2 \quad (1d)$$

$$\rightarrow CH_4 + {}^1O_2 \quad (1e)$$

Reaction (1a) leads to the formation of H atoms through the subsequent fast decomposition of CH_3O. Direct measurements of the rate coefficients for Reaction (1) are not available.

Reaction (−1d) was recently studied experimentally and theoretically at elevated temperatures [3]. The theoretical rate coefficient, which was in good agreement with the accompanying experimental measurements, was higher than previous estimates [4–8] by factors of 3–10. The values for k_{1d} appearing in many popular reaction mechanisms [1,9–13] (summarized in Table 1) are based on the earlier, lower recommendations for k_{-1d} and may be expected to suffer from similar errors.

Baulch et al. [8] recommended $k_{1a} = 3 \times 10^{-11}$ cm^3 molecule^{-1} s^{-1} with an uncertainty of an order of magnitude based on a set of indirect measurements [14]. The reaction mechanisms summarized in Table 1 adopt values for k_{1a} within this range ($1.3–6.3 \times 10^{-11}$ cm^3 molecule^{-1} s^{-1}), but the rate coefficients still vary from one another by as much as a factor of 5. Product channels other than (1a) and (1d) are not expected to be important. Note that the reaction mechanisms summarized in Table 1 predict branching ratios for the $CH_3O + OH$ and $CH_4 + O_2$ products varying from 3:1 to 43:1, and this branching ratio may be important in controlling ignition in high pressure systems.

Scire et al. [1,12] perturbed the well characterized lean moist CO oxidation system with methane in flow reactor experiments, and they used modeling studies to extract rate coefficients for the two major product channels of Reaction (1). Under their conditions and in the absence of CH_4, CO was primarily consumed by OH. At low pressures (~1 atm) and when small amounts of CH_4 were added to the system, CO oxidation was found to be suppressed, as CH_4 consumed OH much faster than CO. At high pressures, however, the addition of CH_4 was found to increase the rate of CO oxidation. The authors identified the $CH_3 + HO_2$ reaction as an important process under these conditions, and the resulting formation of $CH_3O + OH$ explained the increased combustion of CO. A detailed error analysis was performed, and the values they obtained for k_{1a} and k_{1d} have considerably reduced uncertainties relative to previous estimates. Their revised value of k_{1d} is higher than previous estimates, as suggested by the results and analysis given in Ref. [3], and the revised branching ratio (5:1) indicates significantly more formation of $CH_4 + O_2$ relative to earlier reaction mechanisms.

Recently, the hydrocarbon oxidation mechanism of Curran [13] was updated with values for k_{1a} and k_{1d} close to those of Scire et al. This agreement is encouraging, but some uncertainty remains due to the indirect nature of these determinations.

Zhu and Lin previously characterized the CH_3OOH system theoretically [15]. The rate coefficient they obtained for (1a) at 1000 K is ~3 times larger than those of Scire et al. and Curran, as shown in Table 1, but is in good agreement with the GRI-Mech parameterization. The value predicted for (1d), on the other hand, is in good agreement with the recent models and is significantly higher than the earlier reaction mechanism parameterizations. The resulting branching ratio predicted by Zhu and Lin at 1000 K (10:1) is at the low end of the range of branching ratios for the earlier reaction mechanisms, but it is still markedly higher than the branching ratios for the recently revised mechanisms of Curran and Scire et al.

Theoretical predictions of the kinetics of Reaction (1) are complicated by the presence of the $CH_3 + HO_2$ and $CH_3O + OH$ barrierless processes. In the theoretical study of Zhu and Lin, the flux through the transition state for the barrierless channels was evaluated using the rigid rotor and harmonic oscillator (RRHO) approximations, which are of dubious validity for barrierless reactions.

Variable reaction coordinate transition state theory (VRC-TST) [16–18] has been developed to accurately treat barrierless reactions. Its direct implementation, in which the interaction potential of the reacting fragments is evaluated on-the-fly using multireference electronic structure calculations, allows for the efficient computation of quantitatively accurate rate coefficients. In recent studies of systems with as many as eight carbon atoms, the VRC-TST method was shown to be computationally practical and to predict rate coefficients with estimated errors of less than 25% for a series of hydrocarbon radical–radical association reactions [19,20]. The ab initio VRC-TST

Table 1
Rate coefficients for the major products of Reaction (1) at 1000 K (10^{-11} cm^3 molecule^{-1} s^{-1}) and the $CH_3O + OH$ branching fraction P_{1a}

Source	k_{1a}	k_{1d}	P_{1a}
Baulch et al. [8] (review)	2.99	0.26[a]	0.92
Leeds 1.5 [9] (modeling)	2.99	0.07[a]	0.98
Konnov [10] (modeling)	1.33	0.07[a]	0.95
GRI-Mech 3.0 [11] (modeling)	6.28	0.17	0.97
Scire et al. [1,12] (modeling)	2.50	0.53	0.83
Curran [13] (modeling)	1.83	0.60	0.75
Zhu and Lin [15] (theory)	6.42	0.61	0.91
Present theory	1.50	0.43	0.78

[a] The rate coefficient included in the mechanism for Reaction (−1d) was transformed using the thermochemistry in Baulch et al. [8].

method was also recently used to describe the kinetics of the $CH_3 + OH$ association reaction with similar accuracy [21].

In the present study, the direct ab initio VRC-TST method is used to characterize the barrierless processes in Reaction (1). The kinetics of the hydrogen abstraction reactions and the $CH_2O + H_2O$ product channel are treated using variational transition state theory and the RRHO approximation. Pressure dependence and product branching are modeled using master equation (ME) simulations. The methods used here were recently validated for the CH_3OH system, where good agreement was obtained between the theoretical predictions and a wide variety of experiment results [21].

We also consider the thermal decomposition of methylhydroperoxide

$$CH_3OOH \rightarrow CH_3O + OH \quad (2a)$$

$$\rightarrow CH_2O + H_2O \quad (2b)$$

$$\rightarrow CH_3 + HO_2 \quad (2c)$$

which has been previously studied experimentally [22] over a limited temperature range (600–700 K), and these results were adopted in a recent review [8]. The experimental results were assigned considerable uncertainty.

The present calculations are also used to characterize the $CH_3O + OH$ association/decomposition reaction, which is briefly discussed.

2. Theory

2.1. Potential energy surfaces

In the VRC-TST rate calculations for the $CH_3 + HO_2$ and $CH_3O + OH$ reactions, the interaction potential energy surfaces were obtained for

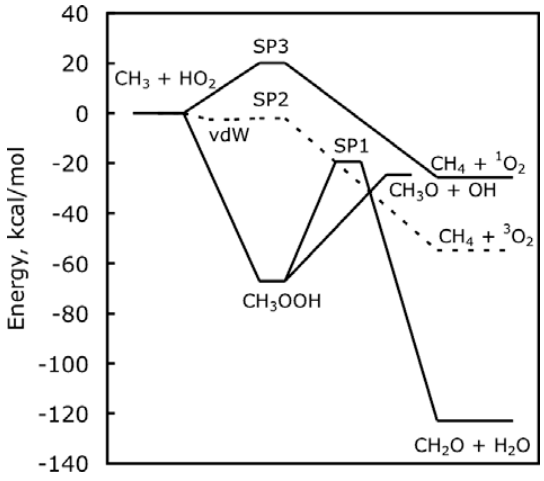

Fig. 1. QCISD(T)/CBS//B3LYP/6-311++G(d,p) channel energies and stationary point energies at 0 K. Energies for the $CH_4 + {}^3O_2$ product channel are taken from Ref. [3].

structures of the reacting fragments fixed at their isolated B3LYP/6-311++G(d,p) [23,24] equilibrium geometries. The remaining degrees of freedom, describing the relative orientation and separation of the fragments, were treated as fully coupled to one another and anharmonic, and the interaction potential was computed on-the-fly using multireference perturbation theory (CASPT2) [25].

The active spaces for the CASPT2 calculations were chosen to be the minimum required to correctly describe the separated fragments: two electrons in two orbitals for the $CH_3 + HO_2$ addition reaction, and six electrons in four orbitals for the $CH_3O + OH$ reaction. To avoid root flipping problems when evaluating the $CH_3O + OH$ interaction energy, orbitals were optimized to minimize the average energy of the four lowest-energy states, which correlate asymp-

Table 2
Reaction enthalpies and stationary point energies at 0 K (kcal/mol)

Reaction	Present[a]	Zhu and Lin[b]	Experiment[c]
$CH_3 + HO_2 \rightarrow$			
$CH_3O + OH$	−24.47	−24.8	-23.8 ± 0.5
$CH_4 + {}^1O_2$	−25.56	−29.4	
$CH_4 + {}^3O_2$	(−54.8)[d]	−58.2	-55.4 ± 0.1
CH_3OOH	−67.11	−70.5	-66.8 ± 1.0
$CH_2O + H_2O$	−122.88	−126.1	-121.7 ± 0.2
$[CH_3OOH \leftrightarrow CH_2O + H_2O]^{\ddagger}$ (SP1)	−19.33	−24.1	
$[CH_3 + HO_2 \leftrightarrow CH_4 + {}^3O_2]^{\ddagger}$ (SP2)	(−1.9)[d]	−0.7	
$[CH_3 + HO_2 \leftrightarrow CH_4 + {}^1O_2]^{\ddagger}$ (SP3)	20.2 (8.8)[e]	4.1	
${}^3[H_3C\cdots HO_2]$ (vdW)	(−2.5)[d]	−1.9	
RMS deviation from experiment	0.8	3.2	

[a] QCISD(T)/CBS//B3LYP/6-311++G(d,p) unless otherwise indicated.
[b] Previous theoretical results [15] obtained using G2M theory.
[c] From Ref. [33].
[d] CCSD(T)/aug-cc-pVTZ//CCSD(T)/aug-cc-pVDZ, from Ref. [3].
[e] CAS+1+2+QC/CBS//CASPT2/aug-cc-pVTZ.

totically with the doubly degenerate $^2\Pi$ state of OH and the doubly degenerate ground state of C_{3v} CH_3O.

The neglect of Jahn–Teller distortion in CH_3O when evaluating the interaction energy simplifies the rate calculations and is not a significant source of error, as discussed elsewhere for the $CH_3O + H$ reaction [21]. Jahn–Teller rovibronic coupling is neglected when evaluating the partition function of the CH_3O reactant. Marenich and Boggs [26] computed thermodynamic functions for the spin-vibronic CH_3O system (including Jahn–Teller and spin–orbit effects), and the enthalpies and entropies they reported differ by no more than 3% from the RRHO estimates used here. Such excellent agreement is likely fortuitous, and larger errors in the RRHO approximation may be expected in general for Jahn–Teller coupled systems.

For the $CH_3O + OH$ reaction, the spin–orbit splitting associated with the $^2\Pi$ state of the OH fragment was included as described in Ref. [21] for the $CH_3 + OH$ reaction. A level shift [27] of 0.3 E_h (1 $E_h = 627.5$ kcal/mol) was applied in all of the CASPT2 calculations. The cc-pVDZ and aug-cc-pVDZ Dunning basis sets [28,29] were used, and basis set convergence of the predicted rate coefficients will be discussed in Section 3.

Stationary point and channel energies on the CH_3OOH potential energy surface were computed using B3LYP/6-311++G(d,p) geometries and QCISD(T) [30,31] energies extrapolated to the complete basis set (CBS) limit [32] using the cc-pVTZ and cc-pVQZ basis sets [28]. QCISD(T)/CBS enthalpies at 0 K, including harmonic B3LYP/6-311++G(d,p) zero-point energy corrections, are shown in Fig. 1 and summarized in Table 2, where they are compared with experimental values [33]. The QCISD(T)/CBS//B3LYP/6-311++G(d,p) energetics are in good agreement with the experimental results, with a root-mean-square error of only 0.8 kcal/mol. Zhu and Lin [15] previously characterized this system using G2M theory [34], and the results are also shown in Table 2. Matthews et al. [35] recently measured the bond dissociation energy of the O–O bond in CH_3OOH to be 42.6 ± 1 kcal/mol, which is in excellent agreement with the present value (42.6 kcal/mol).

The Q_1 diagnostic [36] is used to estimate the importance of multireference effects and thereby the reliability of the QCISD(T) calculations. For most of the species considered here, the Q_1 diagnostic was less than ~0.02, suggesting that the QCISD(T) method is appropriate for these systems. The Q_1 diagnostic for the saddle point for H abstraction on the singlet surface (SP3) was 0.17, indicating that this energy is unreliable and that multireference methods are required for accurately modeling this process, as discussed next.

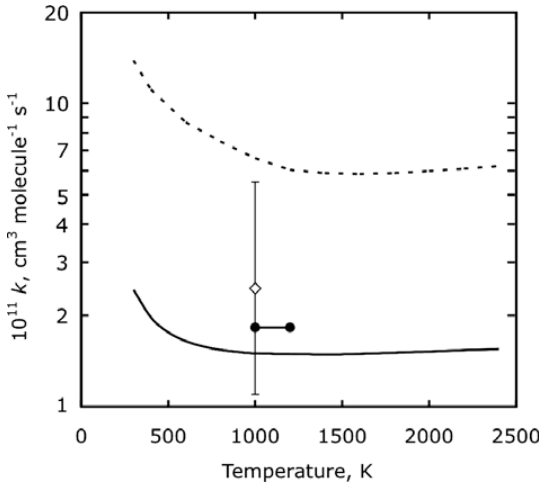

Fig. 2. Present predicted rate coefficient for the $CH_3 + HO_2 \rightarrow CH_3O + OH$ reaction (solid line). The previous theoretical result of Zhu and Lin [15] (dotted line) and values from the recently updated reaction mechanisms of Scire et al. [1,12] (diamond) and Curran [13] (circles) are also shown.

The geometry of SP3 was optimized using the CASPT2/aug-cc-pVTZ method with an active space of 4 electrons and 3 orbitals (4e,3o). These orbitals correspond to the radical orbitals of the A' and A'' ground states of HO_2 and the radical orbital of CH_3. The presence of a low-lying excited state near SP3 required the use of state averaging in the CASSCF orbital optimization step of the CASPT2 calculations. The optimized CASPT2/aug-cc-pVTZ geometry differs significantly from the B3LYP/6-311++G(d,p) geometry. Specifically, the forming (H_3C–HO_2) and breaking (H_3CH–O_2) bond distances predicted by the B3LYP method are 0.2 Å longer and 0.1 Å shorter, respectively, than those predicted by the CASPT2 method. The orientation of the reacting fragments is also significantly different.

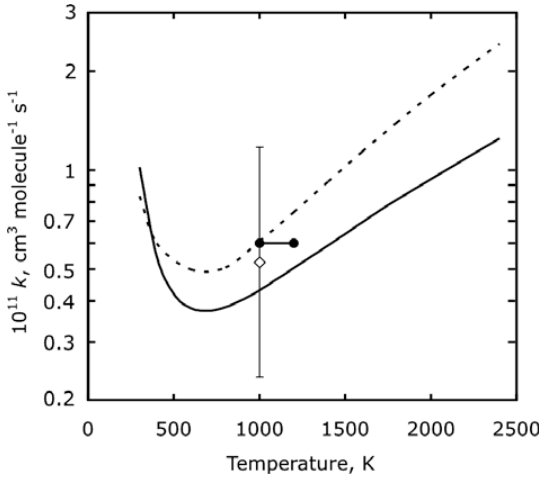

Fig. 3. Rate coefficient for the $CH_3 + HO_2 \rightarrow CH_4 + O_2$ reaction. Symbols are the same as in Fig. 2.

The CASPT2/aug-cc-pVTZ method predicts a C_s structure for SP3, whereas the B3LYP/6-311++G(d,p) saddle point has no symmetry.

The zero-point-inclusive barrier height predicted by the CASPT2/aug-cc-pVTZ method is only 1.8 kcal/mol, which is much lower than the QCISD(T)/CBS//B3LYP/6-311++G(d,p) barrier height reported in Table 2 (20.2 kcal/mol). The QCISD(T)/CBS//CASPT2/aug-cc-pVTZ barrier height is 11.7 kcal/mol, intermediate of the two results. One may question the use of a single reference method (QCISD(T)) for making a high level energy correction for this multireference system. We therefore also performed calculations with the Davidson corrected [37] multireference configuration interaction with singles and doubles (CAS+1+2+QC/CBS//CASPT2/aug-cc-pVTZ) method [38], which predicts a barrier height of 8.8 kcal/mol, in fair agreement with the QCISD(T)/CBS//CASPT2/aug-cc-pVTZ result. We take 8.8 kcal/mol as the best estimate of the barrier height, but we assign this barrier height an uncertainty of 3 kcal/mol. The effect of this uncertainty on the kinetics of Reaction (1e) will be discussed in Section 3.

The saddle point for H abstraction on the triplet surface (1d) could not be located at the B3LYP/6-311++G(d,p) level of theory. The reverse process was previously characterized in detail using CCSD(T)/aug-cc-pVDZ geometries and frequencies and CCSD(T)/aug-cc-pVTZ energies, and good agreement between the predicted and measured rate coefficients over a wide temperature range was obtained in that study [3]. In the present study, we therefore simply adopt the previous theoretical values, transformed via the equilibrium constant obtained using the geometries, frequencies, and energies calculated in Ref. [3].

The Gaussian program package [39] was used to perform the density functional theory calculations and geometry optimizations, and the Molpro program package [40] was used to perform the QCISD(T), CASPT2, CAS+1+2+QC, and spin–orbit calculations.

2.2. Rate calculations

The kinetics of the barrierless $CH_3 + HO_2$ reaction and $CH_3O + OH$ product channel were calculated using the VRC-TST method [16–18], as implemented in the computer code VaReCoF [41]. The geometry dependence of the optimal dividing surface for barrierless reactions may vary significantly as a function of total energy E, total angular momentum J, and temperature. In the present work, several types of dividing surfaces were considered, and the optimal dividing surface for each E,J pair was determined variationally. For both the $CH_3 + HO_2$ and $CH_3O + OH$ reactions, center of mass (CoM) dividing surfaces were included, where these dividing surfaces are defined in terms of a fixed CoM separation varying from 2 to 9 Å. For the $CH_3 + HO_2$ reaction, MF dividing surfaces [42] with pivot points displaced from the carbon atom perpendicular to the plane of the CH_3 fragment and displaced from the terminal O atom perpendicular to the plane of the HO_2 fragment were considered. Test calculations confirmed that MF dividing surfaces are not important for describing the $CH_3O + OH$ reaction, in agreement with previous VRC-TST studies involving the CH_3O and OH fragments [21,43].

The VRC-TST rate calculations were corrected for dynamical recrossing using the transmission coefficient obtained in a previous trajectory study of hydrocarbon radical–radical association reactions. This value was found to be 0.85 and independent of temperature [20].

Rovibronic coupling (i.e., the angular momentum coupling of the electronic and rotational degrees of freedom) in the OH fragment and the $CH_3O + OH$ transition state species was treated as described in a previous study of the $CH_3 + OH$ reaction [21].

The kinetics of the $CH_2O + H_2O$ product channel and the $CH_3 + HO_2 \rightarrow CH_4 + {}^1O_2$ reaction were characterized using the RRHO approximation and microcanonical variational transition state theory. This approach is appropriate for reactions with finite barriers and "tight" transition states. For the $CH_2O + H_2O$ channel, the B3LYP/6-311++G(d,p) method was used to compute the minimum energy path and frequencies, and the QCISD(T)/CBS method was used to determine the energetics. As discussed above, the $CH_3 + HO_2 \rightarrow CH_4 + {}^1O_2$ saddle point (SP3) has significant multireference character, and the CAS+1+2+QC/CBS//CASPT2/aug-cc-pVTZ method was used to obtain energies and frequencies for Reaction (1e). The lowest frequency mode for SP3 was treated as a free rotor.

3. Results and discussion

3.1. $CH_3 + HO_2$ bimolecular reaction

The VRC-TST capture rate coefficient for the $CH_3 + HO_2$ reaction computed using the CASPT2 method and the cc-pVDZ basis set is 10–25% lower than the aug-cc-pVDZ result. Basis set sensitivity was further tested using the basis set correction potential (BSCP) scheme to obtain aug-cc-pVTZ quality results, as discussed elsewhere [19,20]. The BSCP calculations confirm that the capture rate coefficient is well converged at the aug-cc-pVDZ level.

Pressure dependence and product branching for the indirect bimolecular Reaction ((1a)–(1c)) were modeled using ME simulations and the same energy transfer parameters and methods that were

recently used to model the CH_3OH system [21]. Transition state information for the barrierless $CH_3OOH \leftrightarrow CH_3O + OH$ product channel was calculated using the direct VRC-TST method, and these calculations are discussed in more detail in Section 3.3 for the $CH_3O + OH$ bimolecular reaction.

Variational transition state theory and the RRHO approximation were used to obtain transition state information for the $CH_3OOH \leftrightarrow CH_2O + H_2O$ product channel. The $CH_3OOH \leftrightarrow CH_2O + H_2O$ process has a 4-center saddle point [15], as the CH_3 group transfers an H atom to O as the O–O bond breaks. Variational effects are minor, lowering the thermal rate coefficient by ~10% relative to the TST result at the maximum in the electronic energy, due to a displacement of the maximum in the free energy relative to the electronic maximum. Tunneling prefactors computed using the one-dimensional asymmetric Eckhart formula [44] and the multi-dimensional small curvature tunneling (SCT) of Truhlar and co-workers [45] are in excellent agreement with one another, although the SCT method is generally expected to be more accurate. Tunneling increases the rate coefficient for (−1b) by factors of 80 and 1.2 at 300 and 1000 K, respectively. The best present theoretical prediction for k^{∞}_{-1b} was fit to $4.087 \times 10^{-15} (T/298\ \mathrm{K})^{2.679} \exp(-51{,}624\ \mathrm{K}/T)\ \mathrm{cm^3\ molecule^{-1}\ s^{-1}}$ for 1500–3000 K.

Due to the low threshold energies for formation of the $CH_3O + OH$ and $CH_2O + H_2O$ products relative to the $CH_3 + HO_2$ reactant energy, the capture rate coefficient represents the total indirect reaction rate, independent of pressure. The exclusive product channel (>99%) is $CH_3O + OH$ formation for pressures up to at least 1000 atm He. The capture rate may therefore be assigned to channel (1a) [$k_{1a} = 7.679 \times 10^{-12} (T/298\ \mathrm{K})^{0.2688} \exp(346.0\ \mathrm{K}/T)\ \mathrm{cm^3\ molecule^{-1}\ s^{-1}}$ for 300–2500 K].

Abstraction on the triplet surface (1d) was previously characterized theoretically [3], and the resulting rate coefficient is adopted here [$k_{1d} = 6.426 \times 10^{-14} (T/298\ \mathrm{K})^{2.228} \exp(1521\ \mathrm{K}/T)\ \mathrm{cm^3\ molecule^{-1}\ s^{-1}}$ for 300–2500 K and independent of pressure]. Rate coefficients for abstraction on the singlet surface (1e) were computed for the CAS+1+2+QC/CBS//CASPT2/aug-cc-pVTZ potential energy surface. The predicted rate coefficient [$k_{1e} = 7.883 \times 10^{-15} (T/298\ \mathrm{K})^{2.776} \exp(-3088\ \mathrm{K}/T)\ \mathrm{cm^3\ molecule^{-1}\ s^{-1}}$ for 300–2500 K] is a factor of 30 lower than that for abstraction on the triplet surface at 2000 K and is three orders of magnitude lower at 1000 K. There is significant uncertainty in the predicted barrier height (8.8 kcal/mol), as discussed above. An uncertainty of 3 kcal/mol corresponds to errors in the predicted rate coefficient of factors of 5 and 2 at 1000 and 2000 K, respectively. Zhu and Lin [15] predicted a barrier height for (1e) of 4.1 kcal/mol and a rate coefficient that is 20 and 6 times larger than the present prediction at 1000 and 2000 K, respectively. Despite the significant uncertainty in the calculated barrier height for (1e), the present analysis confirms the previous conclusion [15] that abstraction on the singlet surface is not an important product channel for Reaction (1).

Figures 2 and 3 show the temperature dependence of the rate coefficients for the two major product channels ((1a) and (1d)) for Reaction (1). Also shown are values taken from the recently revised mechanisms of Scire et al. [1,12] and Curran [13], as well as the previous theoretical predictions of Zhu and Lin [15]. For k_{1d} at 1000 K, the theoretical values agree well with one another and with the recent updates to the detailed reaction mechanisms. The present value for k_{1a} is within the reported uncertainty of Ref. [1], whereas the previous theoretical prediction of Zhu and Lin is a factor of ~3 higher. The present direct VRC-TST-based calculations performed with high level multireference electronic structure theory potential energy surfaces are expected to be more accurate than the previous RRHO-based theoretical treatment.

The present theoretical analysis provides strong support for the recent revisions of Scire et al. [1,12] and Curran [13] to the rate coefficients for the $CH_3 + HO_2$ reaction. The revised modeling studies and the present theoretical results suggest a branching ratio of ~4:1 in contrast to the earlier reaction mechanism parameterizations and previous theoretical work.

3.2. CH_3OOH dissociation

The competitive dissociation of the CH_3OOH complex was modeled using ME simulations and the transition state information discussed above. The complex has two torsional modes, which were treated as hindered rotors. The H_3C–OOH torsion has a period of 60° and a torsional barrier of 2.75 kcal/mol. The CH_3O–OH torsion has a period of 180° and a torsional barrier of 5.31 kcal/mol. The exclusive product channel for reaction 2 at 500–2500 K and 1–10^5 Torr He is the formation of $CH_3O + OH$. The predicted rate coefficients were fit to Troe forms [46] (see, e.g., the appendix of Ref. [21]) with the parameters $k^{\infty}_{2a} = 5.684 \times 10^{16} (T/298\ \mathrm{K})^{-1.153} \exp(-22{,}270\ \mathrm{K}/T)\ \mathrm{s^{-1}}$, $k^{0}_{2a} = 1.773\,(T/298\ \mathrm{K})^{-7.502} \exp(-23{,}531\ \mathrm{K}/T)\ \mathrm{cm^3\ molecule^{-1}\ s^{-1}}$, and $F^{c}_{2a} = 0.1625 \exp(-T/36{,}562\ \mathrm{K}) + 0.8375 \exp(-T/498.8\ \mathrm{K}) + \exp(-9990\ \mathrm{K}/T)$. Maximum and average unsigned fitting errors were 23% and 12%, respectively. The present results are in good agreement with Zhu and Lin [15] at 1 atm and are within the significant uncertainty assigned to the experimental results of Lightfoot et al. [22], which span

the range 600–700 K. For example, at 1 atm and 700 K, the present result (28.4 s^{-1}) agrees well with that of Zhu and Lin (25.0 s^{-1}) and Lightfoot et al. (39.1 s^{-1}).

3.3. $CH_3O + OH$ bimolecular reaction

The VRC-TST capture rate coefficient for $CH_3O + OH$ association is weakly dependent on basis set, differing by less than 5% for the cc-pVDZ and aug-cc-pVDZ basis sets. The capture rate coefficient represents the high pressure limit, where CH_3OOH is the exclusive product species. ME simulations were carried out to determine pressure dependence and product branching. The formation of CH_3OOH is the major product for 1–10^5 Torr and up to ~1500 K. Rate coefficients may be obtained from the Troe forms given for (2a) in Section 3.2 and the present theoretical equilibrium constant: $K_{2a}^{eq} = 7.979 \times 10^{-28}$ $(T/298\ \mathrm{K})^{1.188} \exp(22{,}350\ \mathrm{K}/T)\ \mathrm{cm}^3\ \mathrm{molecule}^{-1}$ for 500–2500 K.

At higher temperatures, both the $CH_3O + OH \rightarrow CH_3 + HO_2$ $[k_{-1a} = K_{1a}^{eq}\ k_{1a}$; $K_{1a}^{eq} = 8.412\ (T/298\ \mathrm{K})^{-0.4081} \exp(-12{,}613\ \mathrm{K}/T)$ for 500–2500 K] and $CH_3O + OH \rightarrow CH_2O + H_2O$ $[k = 9.042 \times 10^{-16}\ (T/298\ \mathrm{K})^{2.500} \exp(-949.0\ \mathrm{K}/T)\ \mathrm{cm}^3\ \mathrm{molecule}^{-1}\ \mathrm{s}^{-1}$ for 500–2500 K] products become important, and the resulting rate coefficients are reasonably independent of pressure.

The $CH_3O + OH \rightarrow CH_2O + H_2O$ hydrogen abstraction reaction, which might be expected to be an important process, is not considered here, as the present study is mainly interested in characterizing the kinetics of the $CH_3OOH \leftrightarrow CH_3O + OH$ process.

4. Conclusions

A theoretical study of the kinetics of the $CH_3 + HO_2$ bimolecular reaction and the decomposition of CH_3OOH has been performed for a wide range of temperatures and pressures relevant to combustion. Rate coefficients were determined using a combination of ab initio calculations, variational transition state theory, and ME simulations, and comparisons were made with available experimental and previous theoretical results. Agreement between the present values for the rate coefficients for the bimolecular reaction and those obtained in two sets of recent modeling studies is excellent. Rate coefficients for the $CH_3O + OH$ reaction were also presented.

Acknowledgments

This work is supported by the Division of Chemical Sciences, Geosciences, and Biosciences, Office of Basic Energy Sciences, US Department of Energy. The work at Argonne was supported by contract number DE-AC02-06CH11357. Sandia is a multiprogram laboratory operated by Sandia Corporation, a Lockheed Martin Company, for the United States Department of Energy under Contract No. DE-AC04-94-AL85000.

References

[1] J.J. Scire Jr., R.A. Yetter, F.L. Dryer, *Int. J. Chem. Kinet.* 33 (2001) 75–100.
[2] E.L. Petersen, D.F. Davidson, R.K. Hanson, *Combust. Flame* 117 (1999) 272–290.
[3] N.K. Srinivasan, J.V. Michael, L.B. Harding, S.J. Klippenstein, *Combust. Flame* 149 (2007) 104–111.
[4] G.B. Skinner, A. Lifshitz, K. Scheller, A. Burcat, *J. Chem. Phys.* 56 (1972) 3853–3861.
[5] R. Shaw, *J. Phys. Chem. Ref. Data* 7 (1978) 1179–1190.
[6] W. Tsang, R.F. Hampson, *J. Phys. Chem. Ref. Data* 15 (1986) 1087–1279.
[7] D.L. Baulch, C.J. Cobos, R.A. Cox, et al., *J. Phys. Chem. Ref. Data* 21 (1992) 411–734.
[8] D.L. Baulch, C.T. Bowman, C.J. Cobos, et al., *J. Phys. Chem. Ref. Data* 34 (2005) 757–1397.
[9] K.J. Hughes, T. Turanyi, M.J. Pilling, Leeds Methane Oxidation Mechanism, version 1.5, 2001, available at http://www.chem.leeds.ac.uk/combustion/methane.html.
[10] A.A. Konnov, Detailed Reaction Mechanism for Small Hydrocarbons Combustion, version 0.4, 1998, available at http://homepages.vub.ac.be/~akonnov.
[11] G.P. Smith, D.M. Golden, M. Frenklach, et al., GRI-Mech, version 3.0, 2000, available at http://www.me.berkeley.edu/gri_mech/.
[12] J.J. Scire Jr., F.L. Dryer, R.A. Yetter, *Int. J. Chem. Kinet.* 33 (2001) 784–802.
[13] H.J. Curran, Combustion Chemistry Centre Reaction Mechanism, updated values via private communication, 2007, available at http://www.nuigalway.ie/chem/c3/mechanisms.htm.
[14] M.B. Colket III, D.W. Naegeli, I. Glassman, *Proc. Combust. Inst.* 16 (1977) 1023–1039.
[15] R. Zhu, M.C. Lin, *J. Phys. Chem. A* 105 (2001) 6243–6248.
[16] S.J. Klippenstein, *J. Chem. Phys.* 96 (1992) 367–371.
[17] S.J. Klippenstein, *J. Phys. Chem.* 98 (1994) 11459–11464.
[18] Y. Georgievskii, S.J. Klippenstein, *J. Chem. Phys.* 118 (2003) 5442–5455.
[19] L.B. Harding, Y. Georgievskii, S.J. Klippenstein, *J. Phys. Chem. A* 109 (2005) 4646–4656.
[20] S.J. Klippenstein, Y. Georgievskii, L.B. Harding, *Phys. Chem. Chem. Phys.* 8 (2006) 1133–1147.
[21] A.W. Jasper, S.J. Klippenstein, L.B. Harding, B. Ruscic, *J. Phys. Chem. A* 111 (2007) 3929–3950.
[22] P.D. Lightfoot, P. Roussel, F. Caralp, R. Lesclaux, *J. Chem. Soc. Faraday Trans.* 87 (1991) 3213–3220.
[23] A.D. Becke, *J. Chem. Phys.* 98 (1993) 5648–5652; C.T. Lee, W.T. Yang, R.G. Parr, *Phys. Rev. B* 37 (1998) 785–789.
[24] R. Krishnan, J.S. Binkley, R. Seeger, J.A. Pople, *J. Chem. Phys.* 72 (1980) 650–654; T. Clark, J. Chadrasekhar, G.W. Spitznagel, P.v.R. Schleyer, *J. Comput. Chem.* 4 (1983) 294–301.

[25] K. Andersson, P.-A. Malmqvist, B.O. Roos, *J. Chem. Phys.* 96 (1992) 1218–1226;
H.-J. Werner, *Mol. Phys.* 89 (1996) 645–661;
P. Celani, H.-J. Werner, *J. Chem. Phys.* 112 (2000) 5546–5557.
[26] A.V. Marenich, J.E. Boggs, *J. Mol. Struct. (THEOCHEM)* 780–781 (2006) 163–170.
[27] B.O. Roos, K. Andersson, *Chem. Phys. Lett.* 245 (1995) 215–223;
P. Celani, H.-J. Werner, *J. Chem. Phys.* 119 (2003) 5044–5057.
[28] T.H. Dunning Jr., *J. Chem. Phys.* 90 (1989) 1007–1023.
[29] R.A. Kendall, T.H. Dunning Jr., R.J. Harrison, *J. Chem. Phys.* 96 (1992) 6796–6806.
[30] J.A. Pople, M. Head-Gordon, K. Raghavachari, *J. Chem. Phys.* 87 (1987) 5968–5975;
K. Raghavachari, G.W. Trucks, J.A. Pople, M. Head-Gordon, *Chem. Phys. Lett.* 157 (1989) 479–483.
[31] The ROHF-RQCISD(T) algorithm is used for the open shell QCISD(T) calculations. See P.J. Knowles, C. Hampel, H.-J. Werner, *J. Chem. Phys.* 99 (1993) 5219–5227;
P.J. Knowles, C. Hampel, H.-J. Werner, *J. Chem. Phys.* 112 (2000) 3106–3107 (E).
[32] J.M.L. Martin, O. Uzan, *Chem. Phys. Lett.* 282 (1998) 16–24.
[33] A. Burcat, B. Ruscic, Ideal Gas Theromochemical Database with Updates from Active Thermochemical Tables, Table 4, November 28, 2007, available at http://garfield.chem.elte.hu/Burcat/BURCAT.THR. HO_2 data from B. Ruscic, R.E. Pinzon, M.L. Morton, N.K. Srinivasan, M.-C. Su, J.W. Sutherland, J.V. Michael, *J. Phys. Chem. A* 110 (2006) 6592–6601.
[34] A.M. Mebel, K. Morokuma, M.C. Lin, *J. Chem. Phys.* 103 (1995) 7414–7421.
[35] J. Matthews, S. Amitabha, J.S. Francisco, *J. Chem. Phys.* 112 (2005) 221101.
[36] T.J. Lee, A.P. Rendell, P.R. Taylor, *J. Phys. Chem.* 94 (1990) 5463–5468.
[37] S.R. Langhoff, E.R. Davidson, *Int. J. Quantum Chem.* 8 (1974) 61–72.
[38] H.-J. Werner, P.J. Knowles, *J. Chem. Phys.* 89 (1988) 5803–5814;
P.J. Knowles, H.-J. Werner, *Chem. Phys. Lett.* 145 (1988) 514–522.
[39] M.J. Frisch, G.W. Trucks, H.B. Schlegel, et al., *Gaussian 03, Revision C.02*, Gaussian, Inc., Wallingford CT, 2004.
[40] H.-J. Werner, P.J. Knowles, R. Lindh, et al., *MOLPRO*, Version 1, 2006.
[41] Y. Georgievskii, S.J. Klippenstein, *VaReCoF*, Sandia National Laboratories and Argonne National Laboratory, 2006.
[42] Y. Georgievskii, S.J. Klippenstein, *J. Phys. Chem. A* 107 (2003) 9776–9781.
[43] A.W. Jasper, S.J. Klippenstein, L.B. Harding, *J. Phys. Chem. A* 111 (2007) 8699–8707.
[44] H.S. Johnston, J. Heicklen, *J. Phys. Chem.* 66 (1962) 532–533.
[45] D.-H. Lu, T.N. Truong, V.S. Melissas, et al., *Comput. Phys. Commun.* 71 (1992) 235–262;
Y.-P. Liu, G.C. Lynch, T.N. Truong, et al., *J. Am. Chem. Soc.* 115 (1993) 2408–2415.
[46] J. Troe, *J. Phys. Chem.* 83 (1979) 114–126.